Tellus (2006), 58B, 310–318
Printed in Singapore. All rights reserved

TELLUS

The effects of Southeast Asia fire activities on tropospheric ozone, trace gases and aerosols at a remote site over the Tibetan Plateau of Southwest China

By C. Y. CHAN[1,*], K. H. WONG[1], Y. S. LI[1], L. Y. CHAN[1] and X. D. ZHENG[2], [1]*Department of Civil and Structural Engineering, The Hong Kong Polytechnic University, Hung Hom, Hong Kong, China;* [2]*Chinese Academy of Meteorological Sciences, Beijing, China*

(Manuscript received 26 July 2005; in final form 21 February 2006)

ABSTRACT

Tropospheric ozone (O_3), carbon monoxide (CO), total reactive nitrogen (NO_y) and aerosols ($PM_{2.5}$ and PM_{10}) were measured on the southeastern Tibetan Plateau at Tengchong (25.01°N, 98.3°E, 1960 m a.s.l.) in Southwest China, where observational data is scarce, during a field campaign of the TAPTO-China (Transport of Air Pollutants and Tropospheric O_3 over China) in the spring of 2004. Fire maps derived from satellite data and backward air trajectories were used to trace the source regions and transport pathways of pollution. Ozone, CO, NO_y, PM_{10} and $PM_{2.5}$ had average concentrations of 26 ± 8 ppb, 179 ± 91 ppb, 2.7 ± 1.2 ppb and 34 ± 23 and 28 ± 19 $\mu g/m^3$, respectively. The measured O_3 level is low when compared with those reported for similar longitudinal sites in Southeast (SE) Asia and northeastern Tibetan Plateau in Northwest China suggesting that there exist complex O_3 variations in the Tibetan Plateau and its neighbouring SE Asian region. High levels of pollution with hourly averages of O_3, CO, NO_y, PM_{10} and $PM_{2.5}$ concentrations up to 59, 678 and 7.7 ppb and 158 and 137 $\mu g/m^3$, respectively, were observed. The increase of pollutants in the lower troposphere was caused by regional built-up and transport of pollution from active fire regions of the SE Asia subcontinent and from northern South Asia. Our results showed that pollution transport from SE Asia and South Asia had relatively stronger impacts than that from Central and South China on the abundance of O_3, trace gases and aerosols in the background atmosphere of the Tibetan Plateau of Southwest China.

1. Introduction

The widespread air pollution in South and Southeast (SE) Asia, and China is a subject of scientific interest and public concern. In South and SE Asia, forest fires, burning of biomass/biofuels (e.g. wood, dung and agricultural residue) is a major source of air pollutants (UNEP and C[4], 2002). In recent years, several large-scale field campaigns (e.g. Hoell et al., 1997; Lelieveld et al., 2001; Jacob et al., 2003) have been devoted to measure long-range transport of air pollution and outflow of pollution from Asia. These experiments revealed that transport of air pollution from these regions gives rise to extensive air quality degradation with local, regional and global implications. Blake et al. (1997) and Chan et al. (2003b) used organic signatures measured onboard a DC-8 research aircraft during a Pacific Exploratory Mission-West B to show that biomass-burning emissions from SE Asia caused significant enhancements of trace gases in the north western Pacific. Chan et al. (2000) and Chan et al. (2003b) showed that the biomass-burning emissions associated with natural and human activated fires in the Indo-Myanmar region of SE Asia caused substantial enhancements of O_3 in the lower troposphere (2.5–6.0 km) over South China at Hong Kong in each spring season. The ozonesonde measurements during transport and chemical evolution over the Pacific in 2001 showed that such O_3 enhancements were also evident over the Tibetan Plateau at Kunming and to a lesser extent in central-eastern China at Linan (Chan et al., 2003a). Lelieveld et al. (2001) reported high pollution levels over the entire northern Indian Ocean towards the intertropical convergence zone. The researchers found that the enhanced carbon monoxide (CO) concentrations were caused by agricultural burning and biofuel use, while high levels of aerosol resulted from fossil fuel combustion and biomass burning in South and SE Asia.

The Tibetan Plateau is the largest plateau in the world that exerts profound thermal and dynamic influences on local and global climate, and atmospheric circulation of the Asian Monsoon System. Each March and April, an air mass starts to inflow from the Indian Ocean through the Bay of Bengal and the

*Corresponding author.
e-mail: cececychan@polyu.edu
DOI: 10.1111/j.1600-0889.2006.00187.x

Tibetan Plateau towards inland Asia. The water content, physical and chemical properties of the air mass have vital regional influences on the weather and climate of China and East Asia. However, field data of trace gases and aerosols that are chemically and radiatively important for the Tibetan Plateau are scarce. Zhou et al. (1995) and Zou (1996) reported that there is a region of low O_3 over the Tibetan Plateau in summer and there was a decreasing trend of O_3 over the Tibetan Plateau from 1978 to 1991. Zheng et al. (2004) showed with ozonesonde data from the northeastern side of the Tibetan Plateau at Xining (101.45°E, 36.43°N, 2296 m a.s.l) that there was low tropospheric O_3 over the Tibetan Plateau in summer. This was the result of long-range transport of O_3-depleted air from tropical SE Asia and the marine boundary layer of the South China Sea towards the Tibetan Plateau. In a recent modelling study, Li et al. (2005) reported that there was elevated CO and dense clouds over the Tibetan Plateau and Southwest China. The authors suggested that it was the result of trapping of pollutants lifted from Northeast India and Southwest China.

The Transport of Air Pollutants and Tropospheric O_3 over China (TAPTO-China) is a field campaign to measure transboundary transport of air pollution from/across the Eurasia continent and China, and its impact on tropospheric O_3 and pollution outflow to the Pacific (www.cse.polyu.edu.hk/research/taptochina/). During the first phase of the field measurement campaign of the TAPTO-China in the spring of 2004, tropospheric O_3 and its precursors (CO, NO_y) and aerosols over the Tibetan Plateau were measured at the southwestern border of China. The aim is to unveil the characteristics of tropospheric O_3, trace gases and aerosols in the background troposphere of the Tibetan Plateau and to understand the impact of trans-boundary transport of air pollution from South Asia and SE Asia and emissions from China on tropospheric O_3, trace gases and aerosols over the plateau. In this paper, the results are presented and analysed with an emphasis on the impact of the biomass-burning emissions as the result of fires in SE Asia and pollution from South Asia on tropospheric O_3, trace gases and aerosols over the Tibetan Plateau of Southwest China.

2. Experiment

2.1. Pollutant measurement

Tengchong (25.01°N, 98.3°E) is situated on the eastern edge of the Tibetan Plateau, with an average altitude of 1640 m a.s.l. It is located 60 km to the east of the Myanmar border and 750 km to the west of Kunming (Fig. 1), the capital of Yunan province. The measurement site is situated on the top of a mountain, with an altitude of 1960 m a.s.l. It is located 5 km to the south of the ozonesonde launching station. There are small hills and a few small villages surrounding the station. The hills are planted with different types of trees and crops. It is a remote and rural area typical of the relatively undeveloped subtropical western

Fig. 1. Map showing the location of the sampling site and neighbouring countries.

part of China. Surface O_3, CO, NO_y, $PM_{2.5}$ and PM_{10} were continuously measured from 7 April to 24 May, 2004. Ambient air samples were drawn through a PFA Teflon tube with a 3/8″ inside diameter. The sampling inlet was located 3 m above ground level on the rooftop of the station. The other end of the sampling line was connected to a glass-made buffer and a bypass pump drawing air at a rate of 10 l/min. The intakes of the analysers for O_3, NO_y and CO were connected to the buffer. The aerosol analysers were connected to the inlet funnel by a tygon extension line of $^1/_2$ inch inside diameter and 0.5 m long.

Surface O_3 concentration was measured by a 2B Technologies O_3 Monitor, which works on the principle of absorption of ultraviolet light at 254 nm by O_3 molecules. The analyser incorporates corrections due to changes in temperature and pressure in the absorption cell and drift in the intensity of the UV lamp. The detection limit of the analyser is 1.5 ppb. CO and NO_y were measured by an Advanced Pollution Instrumentation, Inc. (API), Model 300E analyser, which is a gas filter correlation, non-dispersive infrared analyser, and a Model 200E chemiluminescene NO_x analyser, respectively. The NO_x analyser simultaneously measures NO and NO_2 concentrations. However, the NO_2 measurement by chemiluminescent method has potential interference from nitric acid, PAN and other atmospheric nitrates. Thus, the NO_x concentrations measured were referred as NO_y instead in this study. The detection limits of the CO and NO_y analysers are about 15 ppb and 0.4 ppb, respectively, for a 5 min average. The analysers were calibrated before and after the field study by an API dynamic dilution calibrator (Model 700) and standard gases traceable to NIST standards. No significant change in the responses of the analysers was seen before and after the observation. The possible baseline drifts of the analysers were checked on a frequency of 2–3 d by standard zero air generated by the calibrator and with the help of an O_3 scrubber supplied by the manufacturer. For the O_3 analyser, zeroing lasted for 15 min. The last 5 min data for each zeroing was taken as the baseline.

The real-time $PM_{2.5}$ and PM_{10} concentrations were measured by portable monitors (DustTrak, TSI Model 8520). The monitor works under the laser photometer principle with light

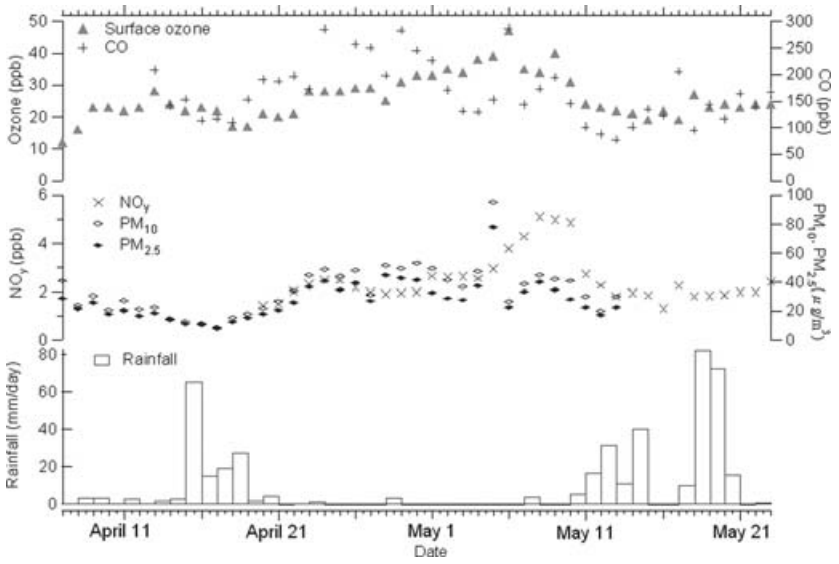

Fig. 2. Daily average concentrations of O_3, CO, NO_y and $PM_{2.5}$ and PM_{10} and rainfall in the sampling period.

scattering technique and in the range of 0.001–100 mg/m^3 (calibrated to respirable fraction of standard ISO 12103–1, A1 test dust). It measures particles size ranging from 0.1 to approximately 10 μm (upper limit is dependent on flow rate). The sampling flow rate is 1.7 L min^{-1}. The concentrations of PM with aerosol diameter less than 2.5 μm and 10 μm ($PM_{2.5}$ and PM_{10}) are distinguished by an impactor installed in the inlet of the monitor. The monitors were calibrated against standard gravimetric samplers (Tapered Element Oscillating Microbalance, TEOM, 1400a) that are specified in the Federal Reference Method (FRM) before deploying the instruments for observation.

2.3. *Satellite images of fire count and backward air trajectory*

We used the fire maps of the SE Asia region of the University of Maryland to identify biomass-burning activity in SE Asia and the South China region (http://maps.geog.umd.edu/products.asp). The fire maps show the spatial distribution of fire spots detected by the MODIS (Moderate Resolution Imaging Spectroradiometer) Rapid Response System using a standard MODIS MOD14 Fire and Thermal Anomalies Product algorithm. The individual detection on the map represents the centre of a 1 km pixel containing at least a fire within that pixel. A detailed description of the fire detection algorithm including the advantages and limitations of the derived data, is available at the University of Maryland website (http://maps.geog.umd.edu/products.asp).

In order to investigate the influence of large-scale motion of air masses on the characteristics of O_3 and other trace gases and aerosols in this region, 3-D backward air trajectories calculated by the National Oceanic and Atmospheric Administration (NOAA) HYSPLIT Model (Draxler and Rolph, 2003; Rolph, 2003) were used to determine the source region of air masses. The input data of the model is from the National Centre of Environmental Prediction (NCEP)'s Global Data Assimilation System. The data has a time resolution of 6 hr, horizontal resolution of 1 degree.

3. Results and discussion

3.1. *Variations of O_3, trace gases and aerosols concentrations*

Figure 2 shows the daily average concentrations of O_3, trace gases and aerosols and Table 1 summarizes their statistics. Ozone, CO, NO_y, and $PM_{2.5}$ and PM_{10} had average hourly concentrations of 26, 179 and 2.7 ppb and 28 and 34 μg/m^3, respectively. They exhibited large variations during the experimental period with lower values at the beginning and the end of the experimental period, and gradual increases in between until they, except CO, reached maximum daily averages of 47 ppb for O_3, 5.1 ppb for NO_y, and 79 and 95 μg/m^3 for $PM_{2.5}$ and PM_{10}, respectively, from 6 to 10 May. The maximum daily average of CO in this period was 287 ppb. The highest daily CO concentrations, 245–308 ppb, were found from 24 to 30 April, when other

Table 1. Measurement statistics of trace gases and aerosols in the sampling period

	Concentrations						Sample no. Days/ hours
	Mean	Std. dev.	Min.	Max.	75%	25%	
O_3 (ppb)	26	8	9	59	31	20	47/1128
CO (ppb)	179	91	23	678	224	113	40/960
NO_y (ppb)	2.7	1.2	0.8	7.7	3.1	1.9	34/816
PM_{10} (μg/m^3)	34	23	0	158	46	17	37/888
$PM_{2.5}$ (μg/m^3)	28	19	0	137	36	14	37/888

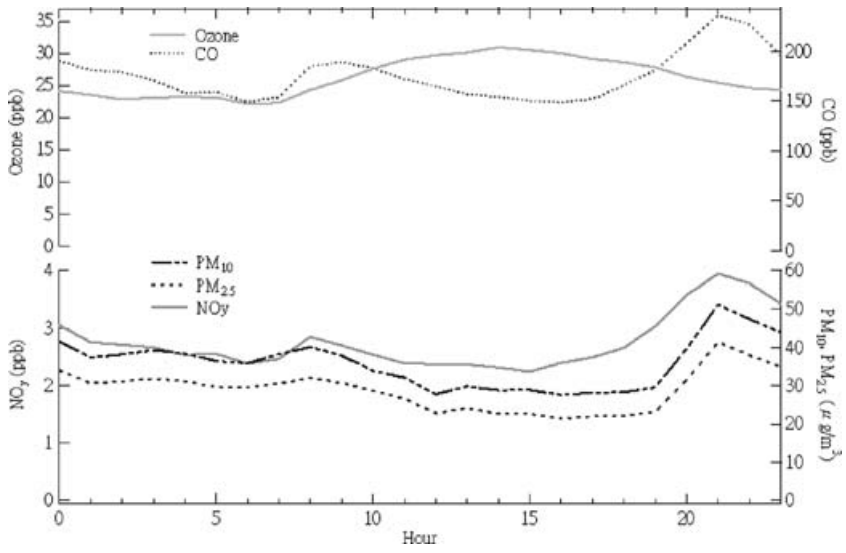

Fig. 3. Average diurnal variations of O_3, CO, NO_y, and $PM_{2.5}$ and PM_{10} concentrations.

species also showed high values. The averaged surface O_3 exhibited a minimum of ∼22 ppb in the morning (6:00) and gradually increases afterwards until it reached a maximum of ∼31 ppb in the early afternoon (14:00) (Fig. 3). It was then followed by a gradual decrease until next morning. CO, NO_y, and aerosols showed a more obvious bimodal pattern with a major peak at late night hours (21:00–22:00) and a minor peak in the morning (8:00–9:00). They showed lower values in the afternoon (15:00–16:00). The daytime increase in O_3 concentration was due to the photochemical O_3 formation from its precursors such as CO, methane and non-methane hydrocarbons in the presence of NO_y and sunlight. The O_3 decrease after the sunset was due to the fact that there was no O_3 being produced and an increase of dry deposition of O_3 in a shallow boundary layer as a result of the radiative cooling of the underlying ground surface, which also caused an accumulation of CO, NO_y and aerosols at night.

The springtime surface O_3, CO, NO_y and aerosols levels over the Tibetan Plateau at Techgchong were low when compared with those reported for other rural and background sites in Asia in the same period of the year. Chan et al. (2002) reported surface O_3 and CO values of 40 and 400 ppb, respectively, for the subtropical South China coast within the Pearl River Delta in Hong Kong. Wang et al. (2001) found that the concentrations of O_3, CO and NO_y were about 50, 600 and 12 ppb, respectively, on the East China coast within the Yangzhi River Delta in Linan. These comparisons suggested that the background air in Southwest China is relatively free of anthropogenic impact compared with that in East and South China. The average concentration of O_3 in Tengchong was also lower than those reported for similar longitudinal sites in tropical Inthanon (18°33′N, 98°3′E, 1450 m a.s.l.) and Srinajarin (14°22′N, 99°07′E, 296 m a.s.l.), Thailand and mid-latitudinal site, Waliguan (36°17′N, 100°54′E, 3810 m a.s.l.) in Northwest China. Pochanart et al. (2001) reported monthly median O_3 concentrations of 33–55 and 28–38 ppb in April and May for Inthanon and Srinajarin, respectively, where active biomass burning occurs. The monthly average O_3 concentrations in the Waliguan Global Atmospheric Watch Station usually range from 50 to 60 ppb in April and May (Tang et al., 1996). The differences in O_3 concentrations in these sites suggest that there exist complex variations of O_3 in the Tibetan Plateau and the neighbouring SE Asian region. Ozone in Tengchong showed comparable values and a similar diurnal pattern to that measured at a tropical coastal site in east India on the Bay of Bengal (Debaje et al., 2003). The measured O_3 and CO were comparable with the mean concentrations of 35 and 125 ppb, respectively, reported for the Northern Hemispheric mid-latitude background air at Mace Head (Derwent et al., 1998) and the values reported for other background sites in the Northern Hemisphere (Oltmans and Levy II, 1994).

3.2. Ozone, trace gases and aerosols concentrations in different air masses

The origins and transport pathways of air mass transport reaching the measurement site can be categorized into three groups based on backward air trajectories. The air masses in the first group were related to the S/SW monsoon and originated from the Bay of Bengal and its surrounding regions. They mostly travelled across Myanmar and sometimes the Myanmar–Bangladesh and Bhutan border and less frequently the northern part of Thailand and Laos before reaching Southwest China (Fig. 4a). In the second group, the air masses traced back to the Central Asian continent. They travelled across northern India and Nepal and Myanmar before entering the border of Southwest China (Fig. 4b). In the last group, the air masses originated from the east. They were either associated with the Northeast Asian monsoon blowing from central and northern China (Fig. 4c) or originated from the region close to the western Pacific and the South China Sea

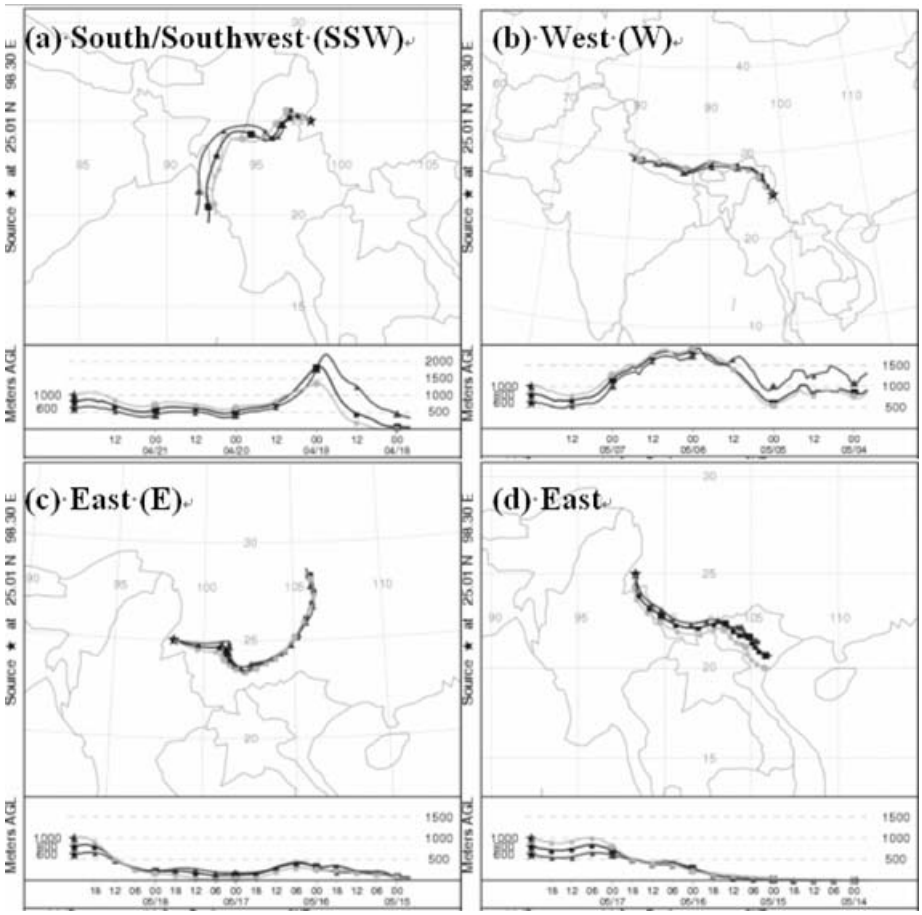

Fig. 4. Representative air trajectories for the three air mass transport groups.

(Fig. 4d). These air masses had to pass over large geographical areas of Central and South China including Yunan, Guizhou, Guangxi and Guangdong to reach the site (Fig. 4c).

Table 2 summarizes the surface O_3, CO, NO_y, and $PM_{2.5}$ and PM_{10} concentrations, daily mean temperature and daily rainfall in the three trajectory groups. The O_3, trace gases and aerosol concentrations associated with the western and southern air masses were higher than those in eastern air masses despite comparable daily mean rainfall in the maritime S/SW and eastern air masses. The higher levels in the S/SW air mass clearly indicated the importance of biomass-burning emissions from fire activities in the SE Asia subcontinent. This will be described in the next section. Interestingly, there were noticeably higher CO and NO_y levels in the continental western air masses. Ozone, $PM_{2.5}$ and PM_{10} levels had the highest concentration in this air mass trajectory. A detailed examination of the trajectory revealed that they were due to the extensive fires occurring in the close vicinity of the western side of Yuanan province in the northern Myanmar and Bangladesh, and northeastern India region, where the air trajectories from the west had passed over (Fig. 4). The fire activities were especially extensive during the period from 21 April to 10 May (Fig. 5).

Table 2. Average concentrations (± standard deviation) of trace gases and aerosols, and meteorological parameters in the three trajectory groups

	ppb			$\mu g/m^3$		Rainfall (mm/d)			Temperature (°C)
	O_3	CO	NO_y	PM_{10}	$PM_{2.5}$	Range	Mean	Median	Mean
South/southwest ($n = 19$)	28 ± 8	161 ± 64	2.3 ± 0.6	37 ± 22	31 ± 17	0–82.7	13.9	0.1	17.8
West ($n = 10$)	30 ± 6	214 ± 55	3.2 ± 1.4	39 ± 10	32 ± 8	0–5.8	1.0	0	18.5
East ($n = 14$)	21 ± 5	151 ± 39	1.9 ± 0.4	21 ± 10	19 ± 7	0.6–72.6	11.3	3.2	14.9

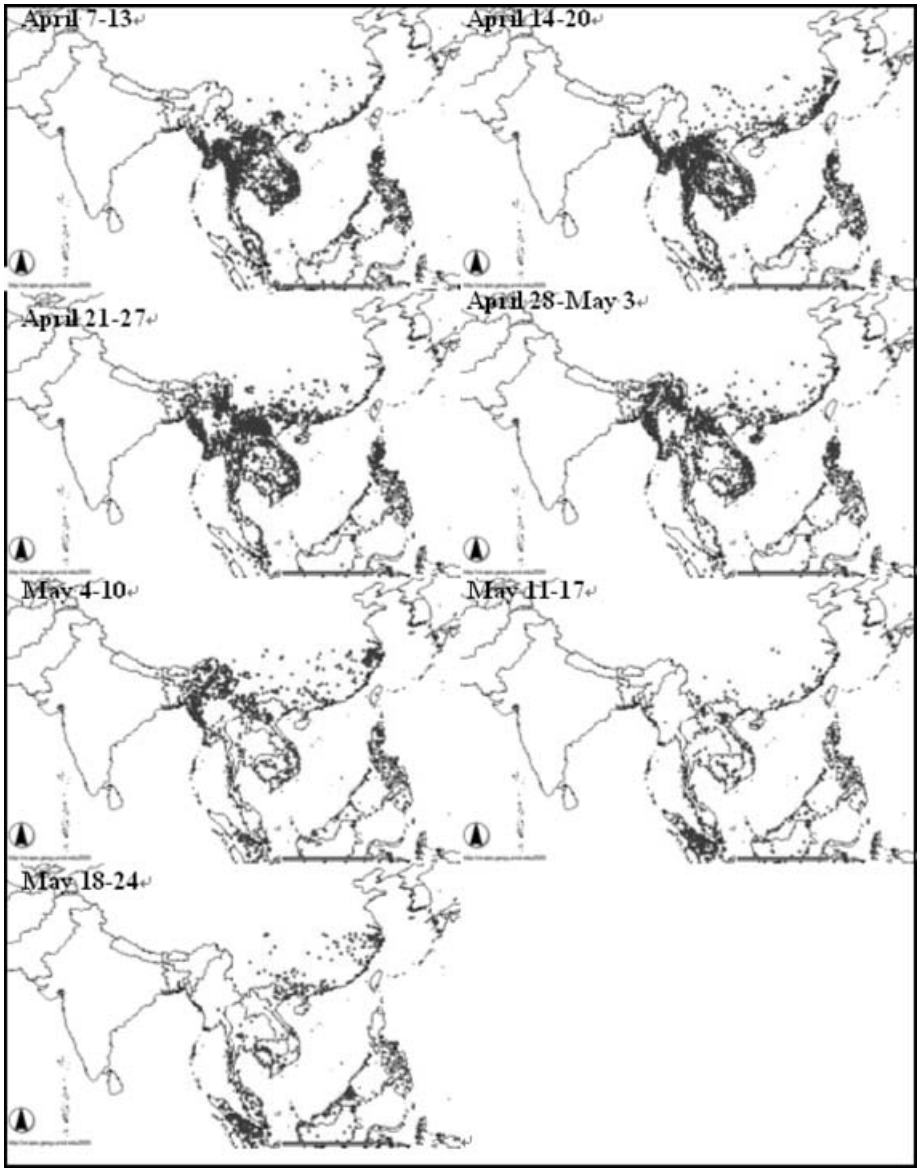

Fig. 5. Geographical distribution of 7 d composite fire hot spots in Southeast Asia derived from MODIS data.

It is surprising to find that relatively lower concentration levels ($O_3 = 21$ ppb, CO = 151 ppb, $NO_y = 1.9$, $PM_{2.5} = 19$ $\mu g/m^3$ and $PM_{10} = 21$ $\mu g/m^3$) were associated with the eastern air masses. The air mass from this direction had to pass through many urban and industrial centres in Central and South China including the Pearl River Delta in Guangdong province. High levels of O_3 and O_3 precursors, such as VOCs and CO, were recorded in the air masses from these regions (Chan et al., 2002 and Wang et al., 2002). Pochanart et al. (2001) also reported low O_3 mixing ratios of 22–26 ppb for the northeastern Asian air mass. The authors believed that the dilution of continental O_3 by the inflow of fresh air from the Indian Ocean and the potential sink of O_3 during transport over the forest area of the tropics (Kirchhoff, 1998) is the reason behind this phenomenon. In our case, we noticed that there were much fewer fires in the eastern neighbour of Tengchong and in the SE and central China (Fig. 5). This is the primary cause of the low pollutants observed in this air mass group. In our case, we noticed that there were few fires in the eastern neighbour of Tengchong (Fig. 5). The air masses transported from the east were associated with rainy weather. In fact, the rainfall record at our sampling site was 0.6–72.6 mm/d in this air mass group. It was raining everyday under this eastern air mass with a median rainfall of 3.2 mm/d, which was much higher than those of S/SW (0.1 mm/d) and western air masses (0 mm/d) (Table 2). The mean temperature was also the lowest in this group (14.9 °C). The unstable atmosphere

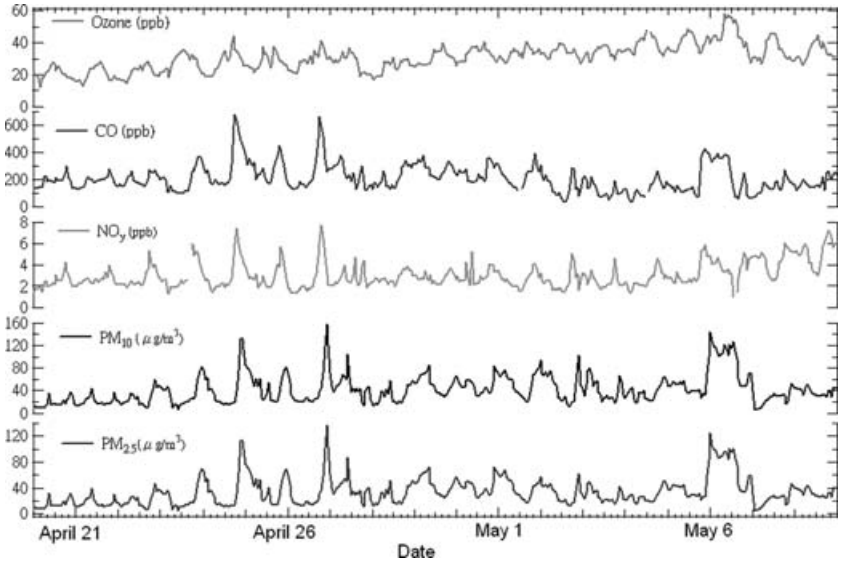

Fig. 6. Hourly concentrations of O_3, CO, NO_y, and $PM_{2.5}$ and PM_{10} from 20 April to 10 May.

associated with rainy weather and lower temperature was not favourable for O_3 formation and pollution accumulation. As a result, a lower pollution level was observed even the air masses had passed over polluted regions. We noted that the mean rainfall in eastern air mass was close to that of S/SW air mass. Yet, the concentrations of O_3, PM_{10} and $PM_{2.5}$ as well as NO_y in S/SW air mass were much higher. This is due to the fact that there were more non-rainy days in the S/SW air mass group with elevated concentration episodes as results of transport of pollutants emitted from the active fire regimes in the south and west directions of Tengchong.

3.3. The effects of fire activities in the SE Asia subcontinent

The large variations of measured O_3, trace gases and aerosols were related to the fire activities in the SE Asia and the region close to the monitoring site. In this part of Asia, climate changes seasonally according to the monsoon flow. The wet season usually starts in May and ends in October whereas the dry season generally begins in November and ends in mid-April. The fire activities, as the result of burning agricultural residues, controlled by these seasonal weather changes, reach their full strength in the dry season in spring. Figure 5 presents the 7 d composite fire count maps for SE Asia derived from the MODIS data (http://maps.geog.umd.edu/maps.asp). In these maps, a hot spot represents a fire that lasted for at least 48 hr. In general, the fire hot spots decreased from April towards May and the hot spots decreased substantially after May. The majority of fires occurred in the SE Asia subcontinent. However, we noted there were suppressed fire activities in the Indo-Myanmar region of northern SE Asia subcontinent and its border to the eastern side of northern India Peninsula prior to 20 April. The fire activities in these regions resumed their strength afterwards until 10 May. The suppressed fire activities in the Indo-Myanmar region in the early period were due to the rainy weather (Fig. 2). In this period, a maximum rainfall of 65.7 mm/d was recorded on 15 April. After that, fine weather prevailed until 10 May when the normal rainy season returned due to the on set of the southwest monsoon. Thus, the lower pollutant levels found at the beginning and end of the experimental periods were due to suppressed fire activities.

The higher pollutant levels in the middle of the experimental period were due to regional build-up of pollution as results of biomass-burning emissions associated with the fire activities. Figure 6 shows the time series of hourly averaged O_3, CO, NO_y and aerosol concentrations from 20 April to 10 May when higher levels of O_3, trace gases and aerosols were observed. Two periods of elevated pollutant levels on 22–28 April and 5–10 May were observed. On 23–28 April, there were sharp increases of CO, NO_y and $PM_{2.5}$ and PM_{10} until they reached the maximum at late night hours every day. The maximum hourly averaged concentrations of CO, NO_y, and $PM_{2.5}$ and PM_{10} reached 678 ppb, 7.5 ppb and 101 and 132 $\mu g/m^3$, respectively, on 24 April and 665 ppb, 7.7 ppb, 137 and 158 $\mu g/m^3$, respectively, on 26 April. High values were also observed on 23 and 25. The peak O_3 concentration occurred in the afternoon most of the time. In the second episode, O_3 precursors NO_y and CO together with aerosols had sharp increases from 18:00 on 5 May. They attained their peak levels at about the late night of 5 May and the early morning of 6 May and sustained their high concentrations until around the early afternoon of 6 May forming a broad high pollutant regime. This phenomenon was unusual when compared with their averaged diurnal variation plotted in Fig. 3. The maximum concentrations of NO_y, CO, and $PM_{2.5}$ and PM_{10} reached 6 ppb, 433 ppb, and 125 and 144 $\mu g/m^3$, respectively,. An O_3 hourly

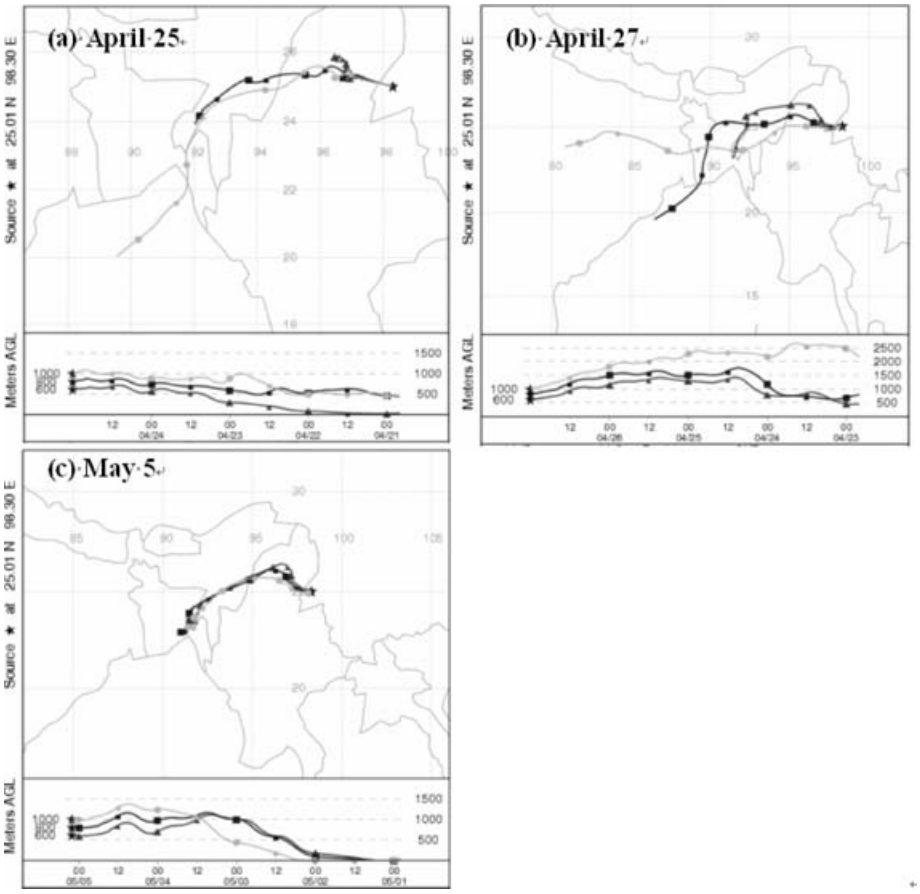

Fig. 7. Five-day backward air trajectories reaching Tengchong at 600, 800 and 1000 m on (a) 25 April, (b) 27 April and (c) 5 May.

maximum of 59 ppb occurred at 10:00 on 6 May. The high O_3 levels sustained until afternoon. The usual O_3 peak occurred at 14:00. After 6 May, CO and aerosols dropped to lower levels. However, the peak concentrations of NO_y and O_3 remained at high levels until 10 May.

Figure 7 shows the 5 d backward air trajectories at the surface layer (600, 800 and 1000 m) on 25 and 27 April, and 5 May when high pollution levels were found. The air masses at the surface originated from the close vicinity of the Bay of Bengal and passed over Bangladesh, Bhutan and Myanmar region in the close neighbourhoods of Tengchong, where active fires were found (Fig. 3). There were upward motions when the air masses passed over these active fire regions. Liu et al (1999), Chan et al. (2000) and Chan et al. (2003b) found that the air masses having passed over these regions had high O_3 as observed over SE China in Hong Kong. The back air trajectory and fire map suggested that it was the result of regional photochemical O_3 formation and accumulation involving the high levels of O_3 precursors during the trans-boundary transport to Southwest China under favourable meteorological conditions.

4. Conclusion

There are limited measurements of tropospheric O_3, trace gases and aerosols in the background atmosphere of tropical and subtropical Asia and China despite the rapid urban, industrial and agricultural development in the region in the last two decades. Our tropospheric O_3, CO, NO_y, and $PM_{2.5}$ and PM_{10} measurements in the spring of 2004 over the Tibetan Plateau in Tengchong showed that the pollutant levels in this relatively undeveloped region of Southwest China were impacted by the biomass-burning emissions associated with fire activities in the SE Asian subcontinent and pollution transport from South Asia. A comparison of the O_3 concentration measured in Tengchong with those in similar longitudinal sites in SE Asia and northeastern Tibetan Plateau suggests that there exist complex variations of O_3 in the Tibetan Plateau and its neighbouring SE Asian region. Back air trajectory analysis revealed that the air masses from the west and south direction that have passed through the Myanmar–Bangladesh region of SE Asia and northeastern India Peninsula of South Asia had the higher O_3, CO, NO_y and aerosols when compared with the air mass associated with the

Northeast Asian monsoon, which had passed over large urban and industrial centres of Central and South China. The findings indicate that the regional built-up of air pollution and transport of the biomass-burning emissions and pollutants from these regions is an important source of trace gases and aerosols in this relatively undeveloped region of western China. We thus concluded that the emissions in SE Asia and South China have relatively stronger impacts than the urban and industrial emissions in the Central and South China on the abundance of trace gases and aerosol in the background atmosphere over the Tibetan Plateau of Southwest China based on the measurement data in the spring of 2004.

5. Acknowledgments

This study is supported by a research grant (A502) from The Hong Kong Polytechnic University and a grant from the Research Grants Council of Hong Kong (PolyU 5048/02 E). We would like to thank the personnel at the Tengchong Meteorological Station for their help in the field experiment. The authors gratefully acknowledge the NOAA Air Resources Laboratory (ARL) for the provision of the HYSPLIT transport and dispersion model and/or READY website (http://www.arl.noaa.gov/ready.html) used in this publication.

References

Blake, N. J., Blake, D. R., Chen, T., Collins, J. E., Sachse, G. W. and co-authors. 1997. Distribution and seasonality of selected hydrocarbons and halocarbons over the western over the western Pacific basin during wintertime. *J. Geophys. Res.* **102**, 28 315–28 333.

Chan, C. Y., Chan, L. Y., Chang, W. L., Zheng, Y. G., Cui, H. and co-authors. 2003a. Characteristics of a tropospheric ozone profile and implications for the origin of ozone over subtropical China in the spring of 2001. *J. Geophys. Res.* **108**, D20, 8800, doi:10.1029/2003JD003427.

Chan, C. Y., Chan, L. Y., Harris, J. M., Oltmans, S. J. and Blake, D. R. 2003b. Characteristics of biomass burning emission sources, transport and chemical speciation of enhanced springtime ozone profile over the troposphere of Hong Kong area. *J. Geophys. Res.* **108**(0), doi: 10.1029/2001JD001555.

Chan, C. Y., Chan, L. Y., Lam, K. S. and Li, Y. S. 2002. Effects of Asian air pollution transport and photochemistry on carbon monoxide variability and ozone production in subtropical coastal south China. *J. Geophys. Res.* **107**, D24, 4746, doi: 10.1029/2002JD002131.

Chan, L. Y., Chan, C. Y., Liu, H. Y., Christopher, S., Oltmans, S. J. and co-authors. 2000. A case study on the biomass burning in Southeast Asia and enhancement of tropospheric ozone over Hong Kong. *Geophy. Res. Lett.* **27**, 1479–1482.

Debaje, S. B., Jeyakumar, S. J., Ganesan, K., Jadhav, D. B. and Seetaramayya, P. 2003. Surface ozone measurements at tropical rural coastal station Tranquebar, India. *Atmos. Environ.* **37**, 4911–4916.

Derwent, R. G., Simmonds, P. G., Seuring, S. and Cimmer, C. 1998. Observation and interpretation of the seasonal cycles in the surface concentrations of ozone and carbon monoxide at Mace Head, Ireland from 1990 to 1994. *Atmos. Environ.* **32**, 144–157.

Draxler, R. R. and Rolph, G. D. 2003. HYSPLIT (HYbrid Single-Particle Lagrangian Integrated Trajectory) model access via NOAA ARL READY website (http://www.arl.noaa.gov/ready/hysplit4.html). NOAA Air Resources Laboratory, Silver Spring, MD, U.S.A.

Hoell, J. M., Davis, D. D., Liu, S. C., Newell, R. E., Akimoto, H. and co-authors. 1997. The Pacific Exploratory Mission-West Phase B: February-March 1994. *J. Geophys. Res.* **102**, 28 223–28 240.

Jacob, D. J., Crawford, J. H., Kleb, M. M., Connors, V. S., Bendura, R. J. and co-authors. 2003. The Transport and Chemical Evolution over the Pacific (TRACE-P) aircraft mission: design, execution, and first results. *J. Geophys. Res.* **108**, 9000, 10.1029/2002JD003276.

Kirchhoff, V. W. J. H. 1998. Surface ozone measurements in Amazonia. *J. Geophys. Res.* **93**, 1469–1476.

Lelieveld, J., Crutzen, P. J., Ramanathan, V., Andreae, M. O., Brenninkmeijer, C. A. M. and co-authors. 2001. The Indian Ocean Experiment: widespread air pollution from South and Southeast Asia. *Science* **291**, 1031–1036.

Li, Q. B., Jiang, J. H., Wu, D. L., Read, W. G., Livesey, N. J. and co-authors. 2005. Convective outflow of South Asian pollution: a global CTM simulation compared with Aura MLS observations. *Geophys. Res. Lett.* **32**(14), L14826, doi:10.1029/2005GL022762, 28 July 2005.

Liu, H., Chang, W. L., Oltmans, S. L., Chan, L. Y. and Harris, J. M. 1999. On springtime high ozone events in the lower troposphere from Southeast Asian biomass burning. *Atmos. Environ.* **33**, 2403–2410.

Oltmans, S. J. and Levy, H. II. 1994. Surface ozone measurements from a global network. *Atmos. Environ.* **28**, 9–24.

Pochanart, P., Kreasuwun, J., Sukasem, P., Geeratithadaniyom, W., Tabucanon, M. S. and co-authors. 2001. Tropical tropospheric ozone observed in Thailand. *Atmos. Environ.* **35**, 2657–2668.

Rolph, G. D. 2003. Real-time Environmental Applications and Display System (READY) Website (http://www.arl.noaa.gov/ready/hysplit4.html). NOAA Air Resources Laboratory, Silver Spring, MD, U.S.A.

Tang, J., Li, X. S. and Zhao, Y. C. 1996. Preliminary analysis on the surface ozone observed at Mt. Waliguan. In: *Variations of Ozone over China and Its Impacts on Climate and Environment (I)* (ed Xiuji Zhou). Meteorological Press, Beijing, China.

UNEP and C^4 (United Nations Environment Programme and Centre for Clouds, Chemistry and Climate). 2002. *The Asian Brown Cloud: Climate and Other Environmental Impacts*. UNEP, Nairobi.

Wang, T., Cheung, V. T. F., Anson, M. and Li, Y. S. 2001. Ozone and related gaseous pollutants in the boundary layer of eastern China: Overview of the recent measurements at a rural site. *Geophy. Res. Lett.* **28**(12), 2373–2376.

Wang, X. M., Sheng, G. Y., Fu, J. M., Chan, C. Y., Lee, S. C. and co-authors. 2002. Urban roadside aromatic hydrocarbons in three cities of the Pearl River Delta, People's Republic of China. *Atmos. Environ.* **36**, 5141–5148.

Zheng, X. D., Zhou, X. J., Tang, J., Qin, Y. and Chan, C. Y. 2004. A meteorological analysis on a low tropospheric ozone event over Xining, northwestern China on July 26∼27, 1996. *Atmos. Environ.* **38**, 261–271.

Zhou, X., Luo, C., Li, W. and Shi, J. 1995. The variation of total ozone in China and unusual ozone depletion center over Tibetan plateau (in Chinese). *Chinese Science Bulletin*, **40**, 1396–1398.

Zou, H. 1996. Seasonal variation and trends of TOMS ozone over Tibet. *Geophy. Res. Lett.* **23**(9), 1029–1032.